Journal of Immunological Methods 473 (2019) 112636

Contents lists available at ScienceDirect

Journal of Immunological Methods

journal homepage: www.elsevier.com/locate/jim

A flexible high content imaging assay for profiling macrophage efferocytosis

Roger Clark[a,*], Laura Usselmann[a], Martin R. Brown[a], Anne U. Goeppert[b], Adam Corrigan[a]

[a] Discovery Sciences, IMED Biotech Unit, AstraZeneca, Cambridge, UK
[b] Precision Medicine, Oncology R&D, AstraZeneca, Cambridge, UK

ARTICLE INFO

Keywords:
High content imaging
Multiparametric
Macrophage
CD14+
Efferocytosis
MerTK

ABSTRACT

Macrophages are a diverse population of cells originating from the myeloid lineage, which form an important component of the innate immune system, helping to regulate immune response through secretion of pro/anti-inflammatory cytokines. However they also have an important homeostatic role – helping to remove cellular debris and apoptotic cells from the body (a phagocytic process known as efferocytosis). Here we describe a robust 384 well microplate based imaging assay, using apoptotic target cells for the specific quantification of efferocytosis in human primary monocyte derived macrophages. The methodology described allows for the assay to run in either fixed end-point or live-cell format (the former offering multiple morphological and intensity-based readouts, whilst the latter opens the possibility for future expansion of the methodology to encompass kinetic profiling). Within the methodology described we couple high content image acquisition (on the Cell Voyager *7000S*) with multi-parametric image analysis - using Perkin Elmer *Columbus* combined with GeneData *Screener*.

1. Introduction

Macrophages as a cell type consist of several specialised sub-populations, each with different protein expression profiles and associated functions. Moreover, these cells show a high degree of plasticity – changing their phenotype readily upon the relevant stimulation (commonly referred to as *polarisation*) (Mosser and Edwards, 2008). The function of specifically polarised macrophages in the clearance of early apoptotic and/or necrotic cellular material (a process known as efferocytosis) is critical for the maintenance of healthy tissue and much work has been done to elucidate the receptors mediating such clearance. The fundamental role for Mer tyrosine kinase (MerTK) in macrophage efferocytosis was shown using MerTK $^{-/-}$ mice (Scott et al., 2001) where ability of macrophages from MerTK $^{-/-}$ animals were compared in their ability to ingest bacteria, latex beads and opsonised particles (along with apoptotic thymocytes). Further to this, other groups have established a role for MerTK in the clearance of apoptotic material by other cell types including retinal epithelial cells (D'Cruz et al., 2000) (Gal et al., 2000) (Duncan et al., 2003), mammary epithelial cells (Sandahl et al., 2010), podocytes (Shao et al., 2010) and Sertoli cells (Sun et al., 2010).

MerTK belongs to a family of related receptor tyrosine kinases known as the TAM kinases (short for **T**yro3, **A**xl and **M**er) (Linger et al., 2008). The TAM kinases are most closely related to RON and c-MET - two other Receptor Tyrosine Kinases (RTK) – although they have quite different functions (Lemke and Rothlin, 2008). The TAMs are all intimately involved in tissue homeostasis within adult humans and their dysfunction is correlated with several disease states (from deficiency leading to chronic inflammation to overexpression linked to poor prognosis in oncology patients) (Lemke, 2013). Indeed several groups have shown that increased MerTK expression in tumour cells and the surrounding stroma correlates with worse prognosis in many tumour types including melanoma, leukaemia, lymphoma, prostate and lung (Graham et al., 2006; Linger et al., 2013; Schlegel et al., 2013; Xie et al., 2015; Graham et al., 2014).

Polarisation of human primary monocyte-derived macrophages with IL-10 and/or dexamethasone has been shown to drive the upregulation of MerTK expression (Zizzo et al., 2012) and further that this phenotype (referred to by Zizzo et al. as 'M2c') specifically mediates the clearance of early apoptotic, as opposed to necrotic cells. MerTK binding to the phosphatidylserine expressed on the outer membrane of apoptotic cells is mediated via one of two known ligands, Gas6 or Protein S, which are themselves secreted by the polarised 'M2c' macrophages (Lemke and Rothlin, 2008; Zizzo et al., 2012). MerTK signalling following binding of its ligand is believed to drive efferocytosis via autophosphorylation of Tyr-867 resulting in activation of the Akt pathway and PKC (Tibrewal et al., 2008). PKC subsequently phosphorylates Focal Adhesion Kinase (FAK) resulting in cytoskeletal

* Corresponding author at: Charles River Laboratories, Chesterford Research Park, Saffron Walden CB10 1XL, UK.
E-mail address: roger.clark@crl.com (R. Clark).

https://doi.org/10.1016/j.jim.2019.112636
Received 2 October 2018; Received in revised form 11 May 2019; Accepted 26 July 2019
Available online 29 July 2019

rearrangement and the engulfment of the bound target cell. The Rho family of GTPases have long been known to be involved in organisation of the actin cytoskeleton and have been shown to be required for phagocytosis in other cell types (Caron and Hall, 1998). MerTK signalling has also been suggested to directly result in activation of RhoA, Rac1 and CDC42 GTPases - mediated by Vav1 (a guanine nucleotide-exchange factor) (Mahajan and Earp, 2003). It is likely that both these pathways work in concert to effect the engulfment of bound target cell material. Engulfed material is taken up into the phagosome, which fuses with a lysosome (forming a phagolysosome) within which an acidic environment and hydrolytic enzymes help to ensure the degradation of engulfed material.

Beyond the key role that MerTK plays in efferocytosis, it has been proposed that signalling via MerTK itself operates a positive feedback loop within the macrophage population, maintaining an anti-inflammatory phenotype through increased Gas6 and IL-10 secretion (Zizzo et al., 2012). Additionally, Tiberwal et al. also suggest that Gas6-MerTK binding downregulates transcription of nuclear factor κB (NF-κB) in a Tyr-867 independent manner, which dampens the secretion of pro-inflammatory cytokines (Tibrewal et al., 2008).

We set out to establish a robust and flexible 384 microplate-based imaging assay for the quantification of macrophage efferocytosis (and the effect of small molecule modulators on this cellular function). The assay was intended to be robust enough for iterative profiling of small molecules, maximising the data generated from precious primary human monocytes. We also wanted to enable a workflow that was flexible enough to allow kinetic or fixed end-point reads.

2. Materials and methods

2.1. Build of an apoptotic Jurkat cell cryobank

Jurkat cells (DSMZ #ACC 282) were cultured in roller bottles at 37 °C, 5% CO_2 using the following media: RPMI 1640 (Sigma #R0883) medium containing 1% L-glutamine (Sigma #G7513), and 10% FBS (Sigma #F7524). Cells were continually passaged, maintaining their density between 2×10^5/ml and 1×10^6/ml in order to yield 1400 ml of suspension at 8.8×10^5 cells/ml (achieved at passage 6). Apoptosis was induced through the addition of 100 nM staurosporine (ApexBio #A8192) to the suspension, returning the cells to the incubator at 37 °C, 5% CO_2 for 2 h. Following treatment with staurosporine, the cell suspension was centrifuged at 300 *g* for 5 mins and the resultant pellet re-suspended in cryopreservation media (10% DMSO (Sigma #D2650), 90% FBS) before being aliquoted into individual cryovials and frozen in a controlled-rate freezer to −150 °C. This resulted in 25 cryovials each containing ~40×10^6 cells/vial.

2.2. Flow cytometry analysis of the apoptotic Jurkat cells

Annexin V binding buffer was made up as follows: 10 mM HEPES (Sigma #H0887), 140 mM NaCl (Sigma #S7653), 2.5 mM $CaCl_2$ (Sigma #C1016), 1:100 dilution of Annexin V-FITC (Molecular Probes #A13199) and 5 μg/ml Propidium Iodide (ThermoFisher #P3566). The buffer was protected from light to avoid photo-bleaching.

1 cryovial of the staurosporine-treated Jurkat cells was thawed and transferred into a total volume of 40 ml HBSS (Sigma #H9394) + 1 mM HEPES (Sigma #H0887) – giving ~1×10^6 Jurkat cells/ml. 5 ml of this Jurkat cell suspension was removed and centrifuged at 300 *g* for 5 mins. The resultant cell pellet was re-suspended in 5 ml of the ***Annexin V binding buffer*** (being careful to minimise any mechanical disruption of the cell membrane). Cells were then incubated at room temperature for 15 mins (in the dark) before being placed on ice and covered to ensure no photo-bleaching of the fluorochromes occurred. Cells were analysed on an LSR Fortessa Flow Cytometer (BD Biosciences, Franklin Lakes NJ) using Excitation 488 nm (Filter 530/30, Mirror 505) and Excitation 561 nm (Filter 610/20, Mirror 600 LP). Data was processed using FlowJo v10 to enable quantification.

2.3. Primary human CD14+ monocyte culture & polarisation

The basic media used for the growth, differentiation and polarisation of CD14+ monocytes / macrophages was as follows: RPMI 1640 (Sigma #R0883) medium containing 1% L-glutamine (Sigma #G7513), 1% Penicillin/Streptomycin (Sigma #P0781) and 10% FBS (Sigma #F7524). Referred to from here onwards as ***Macrophage growth media***.

CD14+ monocytes were obtained from ZenBio (Durham, NC). Cells from two different donors (lot #CD14MC111015C & lot #CD14MC060116A) are referred to within this manuscript as Donor #1 & Donor #2. Cells were thawed directly into pre-warmed ***Macrophage growth media*** (1 ml of cells into 9 ml of media) and immediately spun at 300 *g* in a centrifuge to pellet the cells. Supernatant containing the cryopreservation media was removed and the cells re-suspended in 20 ml pre-warmed ***Macrophage growth media*** and cell number confirmed on a cell counter using Trypan Blue exclusion. 50 ng/ml human recombinant M-CSF (Peprotech #300–25) was added to the cell suspension and the full 20 ml seeded directly into a single T175 cell culture flask (assuming a total cell number of approximately 5×10^6 cells). The flask was incubated at 37 °C, 5% CO_2 for 4 days.

Following 4 days of differentiation, the media was exchanged for 20 ml of fresh pre-warmed ***Macrophage growth media*** supplemented with one of the following polarising conditions (dependent on the experiment) referred to from here on as ***Polarisation media***:

a. 10 ng/ml recombinant human IFNγ (R&D Systems #285-IF) + 1 μM LPS (Sigma #L5293)
b. 50 ng/ml recombinant human M-CSF (Peprotech #300–25)
c. 50 ng/ml recombinant human IL-10 (Peprotech #200–10)
d. 50 ng/ml recombinant human IL-10 (Peprotech #200–10) + 100 nM Dexamethasone (Sigma #D4902)

The flask was then returned to the incubator at 37 °C, 5% CO_2 for a further 2 days. ***Polarisation media (d) was used for the finalised assay conditions***.

2.4. CellTracker staining & plating of macrophages

CellTracker staining media was made up as follows: RPMI 1640 (Sigma #R0883) medium containing 1% L-glutamine (Sigma #G7513) and 1% Penicillin/Streptomycin (Sigma #P0781).

Following polarisation for 2 days, the media was exchanged for 20 ml of pre-warmed ***CellTracker staining media*** containing 1 μM *CellTracker Deep Red* (Molecular Probes #C34565). The flask was returned to the incubator at 37 °C, 5% CO_2 for 30 min. Following incubation with *CellTracker* dye, the staining media was removed to waste. Cells were dissociated from the growing surface by addition of 3 ml *TrypLE* (Gibco #12604013) and incubation at 37 °C, 5% CO_2 for 5 min. Following the incubation, the flask was tapped firmly to lift the macrophages from the surface and the *TrypLE* reaction stopped through the addition of 17 ml of pre-warmed ***Polarisation media***. The cell suspension was counted and diluted to 1.5×10^5 cells/ml in ***Polarisation media***. 40 μl of cell suspension was added to each test well of a 384 *CellCarrier Ultra* microplate (PerkinElmer #6057308) using a MultiDrop Combi (ThermoFisher, Waltham MA) resulting in 6000 cells/well. Microplates were lidded and placed in a rotating incubator at 37 °C, 5% CO_2 overnight.

2.5. Test compound (or blocking antibody) addition to microplates

Following overnight incubation, 120 nl of test compound in 100% DMSO (Sigma #D2650) was dispensed directly into the test wells of each microplate across a dose range (resulting in a final DMSO concentration of 0.3%), using an *Echo 555* acoustic dispenser (Labcyte, San

Jose CA). Control wells were also dispensed using the *Echo 555* as follows:

Minimum efferocytosis control: 120 nl *Cytochalasin D* (CytoD) (Gibco #PHZ1063) in 100% DMSO (Sigma #D2650) to result in a final test concentration of 3 μM in 0.3% DMSO.

Maximum efferocytosis control: 120 nl of 100% DMSO (Sigma #D2650) to result in a final test concentration of 0.3% DMSO.

For the MerTK blocking antibody experiments either Goat anti-Human MerTK (R&D Systems #AF891) or normal Goat IgG isotype control (R&D Systems #AB-108-C) was used at a concentration of 20 μg/ml.

Microplates were lidded and returned to the incubator at 37 °C, 5% CO_2 for 1 h.

2.6. Jurkat cell staining & addition to microplates

Jurkat suspension buffer was made up as follows: HBSS (Sigma #H9394) + 1 mM HEPES (Sigma #H0887).

A cryovial of the apoptotic Jurkat cells was thawed and the full contents (1 ml suspension) was transferred into 9 ml of pre-warmed ***Jurkat suspension buffer*** and centrifuged at 300 *g* for 5 min. The supernatant was removed and the resultant pellet re-suspended to a concentration of 1.5×10^6 cells/ml. 1 μM *pHrodo Red SE* (ThermoFisher #P36600) was added and the cell suspension incubated at room temperature (in the dark) for 30 min. Following incubation the cell suspension was centrifuged at 300 *g* for 5 min and the resultant pellet re-suspended in fresh ***Jurkat suspension buffer*** to achieve a concentration of 7.5×10^5 cells/ml.

Following completion of the macrophage incubation with test compound, 20 μl of pHrodo stained Jurkat cells were added directly to the test wells of the microplates (resulting in 15,000 Jurkat cells per well; a 1:2.5 ratio of macrophages to Jurkat cells). The microplates were lidded and spun briefly in a centrifuge (pulsing to 150 *g*) to bring the Jurkat cells to the base of the well. Microplates were returned to the incubator at 37 °C, 5% CO_2 for 1 h.

2.7. Cell fixation & MerTK staining

Methanol-free paraformaldehyde was made up at 8% in water and frozen in aliquots for later use.

Following incubation of the macrophages with the Jurkat cells, cells were fixed by the addition of 60 μl of 8% paraformaldehyde to each of the test wells on the microplates, using a Multidrop Combi. Microplates were re-lidded and incubated at room temperature for 30 min (in the dark). Microplates were washed using an *EL406* plate washer (BioTek, Winooski VT) using a gentle 'rolling-wash' dispensing 2× cycles of 120 μl of fresh PBS whilst continuously aspirating – to avoid excessive cell loss from dispensing directly into dry wells. The test wells were left with 40 μl of fresh PBS covering the cells and plates were sealed with black adhesive plate-seals.

For MerTK staining experiments (Fig. 2) macrophages – without addition of Jurkat cells - were fixed and washed in the same way as described above, however following the wash step PBS was aspirated from the wells using the same *EL406* plate washer. ***Blocking buffer*** was made up as follows: PBS containing 0.1% Triton X-100 (Sigma #T8787) and 2% BSA (Sigma #A2153). 30 μl of this ***Blocking buffer*** containing a 1:1000 dilution of 10 mg/ml Hoechst 33342 solution (Invitrogen #H3570) was added to the test wells using a Multidrop Combi and the plates incubated at room temperature for 45 min. Microplates were washed using an *EL406* plate washer with the same gentle 'rolling-wash' described above, aspirating the remaining PBS at the end. 20 μl of rabbit anti-human MerTK antibody (CST #D21F11) at 1:500 dilution in ***Blocking buffer*** was added to the test wells using a Multidrop Combi and the plates incubated overnight at 4 °C. Microplates were washed using an *EL406* plate washer with the same gentle 'rolling-wash' described above aspirating the remaining PBS at the end. 20 μl of Alexa Fluor 488 (AF488) donkey anti-rabbit antibody (Invitrogen #A21206) at 1:1000 dilution in ***Blocking buffer*** was added to the test wells using a Multidrop Combi and the plates incubated at room temperature for 1 h. Finally microplates were washed using an *EL406* plate washer with the same gentle 'rolling-wash' described above leaving the wells containing 40 μl of fresh PBS, before plates were sealed with black adhesive plate-seals.

2.8. Image acquisition

Microplates were imaged on a *CellVoyager 7000S* (Yokogawa, Musashino Tokyo) high-throughput confocal imager containing a 5.5 megapixel Andor Neo sCMOS camera (Oxford Instruments, Abingdon UK).

For live-cell imaging the 'live-cell chamber' on the CV7000S was employed to ensure that the microplate was maintained at 37 °C, 5% CO_2 within the instrument. A single image was acquired for each test well at 4× magnification on a single fluorescent channel (*pHrodo Red SE* – Jurkat cells): Ex 561 nm | Em 600/37.

For fixed-cell imaging confocal images were acquired at 20× magnification using a long working distance objective, (Olympus LUCPLFLN 0.45 NA, WD 6.6–7.8 mm) on 2 fluorescent channels for each test well over 9 fields of view, using 2 × 2 binning for each channel:

Channel #1 (CellTracker Deep Red - Macrophages):
Ex 640 nm | Em 676/29.
Exposure time: 50 ms.
Z Offset: −4 μm.
Channel #2 (*pHrodo Red SE* – Jurkat cells):
Ex 561 nm | Em 600/37.
Exposure time: 15 ms.
Z Offset: −3 μm.

For fixed-cell imaging of the MerTK stained cells (Fig. 2) confocal images were acquired at 20× magnification on 3 fluorescent channels for each test well over 4 fields of view, using 1 × 1 binning for each channel:

Channel #1 (Hoechst - Nuclei).
Ex 405 nm | Em 445/45.
Exposure time: 50 ms.
Z Offset: −5 μm.
Channel #2 (AF488 - MerTK):
Ex 488 nm | Em 525/50.
Exposure time: 50 ms.
Z Offset: −5 μm.
Channel #3 (CellTracker Deep Red - Cytoplasm):
Ex 640 nm | Em 676/29.
Exposure time: 20 ms.
Z Offset: −5 μm.

2.9. Image analysis

Live-cell images were analysed in *Columbus* (PerkinElmer, Waltham MA) to generate a single intensity measure per well (***Whole_Well_pHrodo_Intensity_Script*** included in supplementary material). For this analysis it was not necessary to segment individual cellular objects as the increase in pHrodo intensity of stained Jurkat cells over the background intensity was large.

Fixed-cell images were analysed in *Columbus* (PerkinElmer, Waltham MA) to generate a number of morphological and intensity-based parameters (Fig. S3, S4 + ***Macrophage_Jurkat_Uptake_Script*** included in supplementary material). For this analysis both macrophages and Jurkat cells were segmented using the CellTracker and pHrodo staining respectively in order to accurately quantify the number of engulfed Jurkat cells per macrophage. We have also provided an orthogonal image analysis algorithm written in *MATLAB* (MathWorks, Natick MA) and included the full code within the supplementary

material (Fig. S5 + ***MatlabCode***) in order to assist groups without access to the *Columbus* package.

3. Calculations and statistics

All data generated from the *Columbus* image analysis was parsed into the *Screener* analysis package (Genedata AG, Basel) for further refinement and analysis. Compound efficacy against two of the primary end-points (efferocytosis and cell number) was determined via measurement of an IC_{50} value using a smart fitting model within *Screener*. Morphological effect was determined using a *Lowest Effective Concentration* calculation (LEC) within *Screener* – establishing the concentration at which the macrophage cell area increased/decreased by > 5 standard deviations from the median of the neutral controls on the microtitre plate (Fig. S6). Compound curves presented in this manuscript have been re-plotted to publication quality within *Prism* (GraphPad, San Diego CA) using equivalent fitting constraints to those used within *Screener*.

Robust Z' (*R Z'*) was calculated within the *Screener* analysis package using the following formula (where RSD = Robust Standard Deviation and RM = Robust Mean)

$$\boldsymbol{RZ'} = 1 - \frac{3^{*}(\mathrm{RSD}_{Max} + \mathrm{RSD}_{Min})}{(\mathrm{RM}_{Max} - \mathrm{RM}_{Min})}$$

Statistical tests performed on the data were 2 tailed *t*-tests (2 sample – equal variance) performed within Microsoft Excel. *P* values in individual figures are indicated as follows:

* indicates $p < .05$, ** indicates $p < .01$, *** indicates $p < .001$, and **** indicates $p < .0005$.

All error bars shown indicate standard deviation of the mean.

4. Results

4.1. Apoptotic Jurkat cell cryobank is predominantly Annexin V + ve/PI -ve

Jurkat cells are an immortalised human T-Lymphocyte line and were selected for use as the apoptotic target cells in this work following their successful application by others in previous published work (Santulli-Marotto et al., 2015; Xu et al., 2006). As this is a suspension line the manipulation of this for generation of the apoptotic cryobank and subsequent addition to test wells containing the adherent macrophages is much easier within a profiling assay context. In development of this assay for the purposes of regular compound profiling our goal was to minimise variability between assay occasions as much as possible and to this end we built our screening-scale cryobank of apoptotic cells at the outset of assay development; this was particularly important as we expected variability would be likely to arise from CD14+ monocytes from different donors and therefore hoped to control this variability as much as possible through consistency with the apoptotic target cells.

As can be seen from Fig. 1A, the Jurkat cell cryobank at point of recovery shows 5% of cells in the dead population (Q2: PI +ve | Annexin V + ve) with an approximate 5/95 split between 'live' (Q4: PI –ve | Annexin V –ve) and 'early apoptotic' (Q3: PI –ve | Annexin V + ve). As expected, there is a blend of cells between the Q4-Q3 populations, however analysis of the Jurkat cells following a further hour of treatment with staurosporine shows that, whilst there is a minimal shift of the population from Q4 to Q3, there is little increase in the dead population within Q2 (Fig. 1B). These results indicate that the Jurkat cell cryobank remained at an early apoptotic stage (with surface expression of phosphatidylserine but retaining membrane integrity) throughout the course of the assay.

4.2. Polarisation conditions selected show a marked increase in MerTK expression

Various polarisation conditions were tested as described in previous published literature (Mosser and Edwards, 2008; Zizzo et al., 2012; Wang et al., 2014) with surface expression of MerTK determined via immunofluorescence imaging. As expected, polarising macrophages with IFNγ + LPS (Fig. 2A, E) resulted in no detectable levels of MerTK expression as the cells are pushed towards a pro-inflammatory phenotype. Hoechst staining confirmed that macrophages remained within the well. Refreshing the M-CSF after 4 days differentiation (Fig. 2B, E) resulted in a slight increase in MerTK expression, although this expression was inconsistent across the cell population. Polarisation with IL-10 (Fig. 2C, E) resulted in a large increase in MerTK expression seen across the majority of cells in the population, however the highest MerTK expression levels were observed with a combined polarisation using IL-10 + Dexamethasone (Fig. 2D, E). As our intention was to generate a consistent macrophage population with high MerTK expression in order to drive a more robust efferocytosis assay for higher throughput profiling, IL-10 + Dexamethasone were selected to polarise M-CSF differentiated macrophages for use in the assay.

4.3. pHrodo signal increases dramatically over 1 h incubation of apoptotic Jurkat cells with macrophages

pHrodo-SE is a cell-permeant rhodamine based dye, which is highly sensitive to pH (the fluorescence intensity dramatically increasing as the pH decreases). This property makes it an ideal tool for phagocytosis / efferocytosis assays as the pH within the phagolysosome is low therefore causing a rapid increase in observed fluorescence as stained objects are engulfed and move into this acidic environment.

To determine an appropriate time-point at which to measure an effect on efferocytosis, the assay system was run in a live-cell kinetic mode, utilising the 'live-cell' chamber available on the *CV7000S*. In this setting we ideally needed to acquire data for all wells across the test plate extremely rapidly to minimise any incubation time difference between the first and last well captured, and therefore made use of the large sCMOS camera on the *CV7000S* combined with a low magnification 4× objective lens. As such an entire well could be acquired in a single field of view which reduced the read time for a whole 384 microplate to < 5 min. The trade-off for this increased speed of acquisition was a decrease in image resolution compared to using the 20× objective, however this was not problematic in this setting due to the high intensity of the pHrodo stained cells once within live macrophages, when combined with an analysis script reporting changes in whole-well intensity (as described in methods 2.9). Images were acquired at various time-points following pre-incubation with either CytoD (a potent inhibitor of actin polymerisation) or 0.3% DMSO vehicle control, followed by addition of the stained Jurkat cells - as defined in methods section. Fig. 3 shows the rapid increase in pHrodo fluorescence intensity observed between 20 min and 50 min at which point the intensity increase starts to flatten out. From this data we selected a 1 h incubation time of Jurkat cells with macrophages for use in the fixed-cell assay. As pHrodo is not marketed as a fixable stain, the drop in intensity seen post cell fixation was unsurprising, however the window observed between DMSO and CytoD control wells was still large and therefore we considered that use of the pHrodo stain would confer an advantage for the assay in determining engulfed versus free Jurkat cells even when used in a fixed end-point assay. The fact that the pHrodo signal appeared to remain fairly stable for up to 4 days (when stored at 4 °C) was also important to consider for an assay to be used in regular compound profiling – the flexibility to cope with unexpected equipment down-time enabled by this assay stability meant that we were confident in maximising the data generated from the precious primary monocytes.

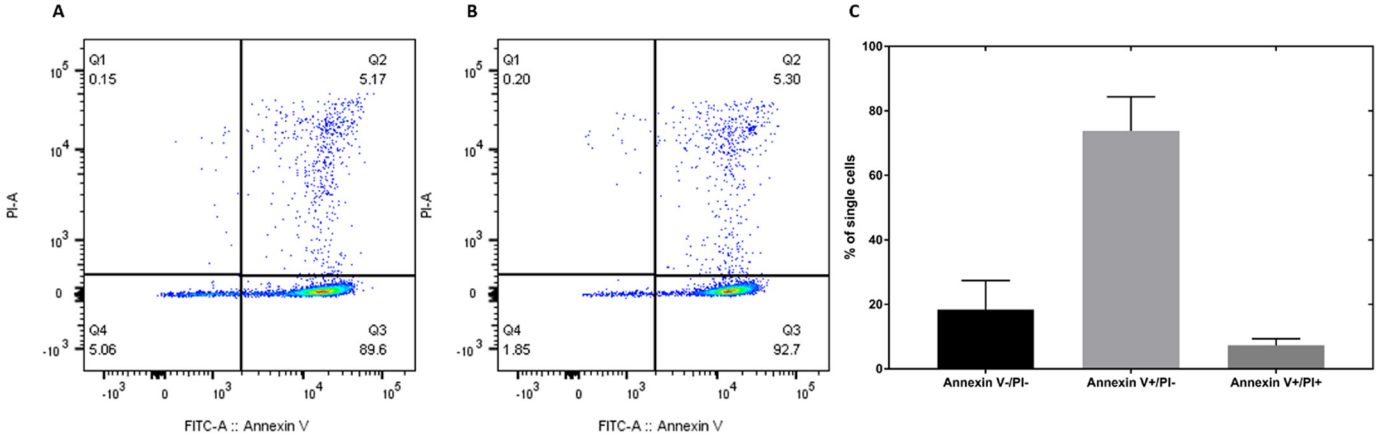

Fig. 1. Flow cytometry analysis of the Apoptotic Jurkat cell cryobank. (**A**) Staurosporine-treated Jurkat cells – as defined in methods 2.1 – cryopreserved, recovered and stained with Annexin V + Propidium Iodide as defined in methods 2.2. (**B**) Jurkat cells treated as those shown in (A) but with an additional 1 h treatment with Staurosporine prior to cryopreservation. (**C**) Quantification of data shown over Q2-Q4 in 1A (n = 4).

4.4. Efferocytosis observed is MerTK dependent

It has been previously reported that efferocytosis in high MerTK expressing macrophages can be inhibited via MerTK antibody to the extracellular domain (Zizzo et al., 2012). In order to establish that our assay was indeed MerTK driven we used the same antibody cited by the authors to validate our system. Fig. 4A shows the effect of the goat anti-human MerTK antibody on the percentage of macrophages classified as 'Efferocytosis positive' within our image analysis algorithm (see supplementary material for details). The percentage of cells classified as 'Efferocytosis positive' (having > 0 engulfed Jurkat cells) was not driven as low as the CytoD control, however CytoD exhibited such a potent effect on the macrophage's ability to remodel its cytoskeleton (and thereby extend pseudopodia to capture target cells) that this was not a surprising result.

4.5. Profiling small molecule inhibitors

Ultimately the purpose of this assay was to enable the profiling of small molecules against macrophage function and as such our final point of assay validation was to test a number of molecules with literature precedent activity against MerTK, related TAM members or the closely related RTK c-MET. Five literature precedent molecules were selected (Fig. 5) for their reported activity against TAM family members or related RTKs:

Compound #1 is reported as a potent and selective inhibitor of the TAM family and c-MET (Kim et al., 2017).

Compound #2 is reported as a potent inhibitor of AXL with similar binding affinity to other TAM family members (Tan et al., 2016).

Compound #3 is reported as a potent inhibitor of c-MET, AXL, MerTK, FLT3 with additional activity against a number of other kinases (Yan et al., 2013).

Compound #4 is reported as a dual MerTK/FLT3 inhibitor (Minson et al., 2014)

Compound #5 is reported as a dual FLT3/AXL inhibitor (Mori et al., 2017)

Along with the 5 molecules shown, some undisclosed AstraZeneca compounds were also tested (selected for various reasons of kinase selectivity/promiscuity and general cell health/toxicity benchmarking). Results gained for the 5 test compounds – along with 1 undisclosed AstraZeneca compound - from multiple test occasions (combining data from different donors) are shown in Table 1. The range of IC_{50} values obtained indicate that the assay was able to distinguish between drugs of different potencies against MerTK driven efferocytosis. Compound #1 was by far the most potent against efferocytosis within our assay, showing ~10 fold increased potency over the structurally related Compound #2. Compound #5 showed no activity within our assay, helping to further validate that the efferocytosis measured within our system is MerTK driven.

Compound #6 is included because whilst it showed micromolar potency against efferocytosis and no effect on overall cell number, it did show an effect on macrophage morphology, the second key assay endpoint. The morphological effects driven by Compound #6 were observable at higher test concentrations, and became very pronounced at 3 μM – 30 μM (Fig. 6A&B). This differing cellular shape, even within cells polarised in the same fashion, made segmentation challenging. Segmentation of fixed cells was achieved by combining a whole cell stain (CellTracker) and a tuneable segmentation algorithm built using *Columbus* (see supplementary material for details). Fig. 6C shows the importance of correct cellular segmentation, as the arrow indicates a Jurkat cell that is on the macrophage surface rather than internalised – through good segmentation this Jurkat cell is excluded from further analysis. Figs. S3 and S4 demonstrate that macrophages of various morphologies are successfully segmented by the Columbus analysis script deployed in this assay. Cytochalasin D is shown for comparison within Table 1; as expected a strong effect can be seen with this compound on both efferocytosis and morphology (CytoD causing rounding of the macrophages rather than spreading, Fig. 6C). Of the compounds tested (including CytoD) none appeared to have an effect on morphology without a corresponding effect on efferocytosis, however given the nature of efferocytosis as a cellular process involving dynamic changes in morphology this is unsurprising. None of the compounds shown in Table 1 caused a detrimental effect to overall macrophage number over the concentration range tested (half-log dilutions from 30 μM over a 12 point curve).

Compound activity in the assay was also assessed against CD14+ monocytes from 2 different donors (Fig. 7A, B) and showed very good correlation in activity. Along with comparison between donors, the same test plates were read in both the live-cell and fixed end-point assay configuration (live-cell read taken at 60 min post Jurkat cell addition). Whilst compounds showing no morphological effect (such as Compound #3) had close alignment of potency against efferocytosis between the two assay configurations (Fig. 7C), compounds driving a morphological effect (such as Compound #6) showed an apparent increase in efferocytosis within the live-cell assay until the reported LEC for morphological effect – resulting in a bell-shaped curve (Fig. 7D). The effect observed with Compound #6 in the live-cell assay configuration was likely an artefact driven by off-target effects on macrophage health, perhaps resulting in localised extracellular regions of lower pH (which would increase the intensity of pHrodo stained Jurkat

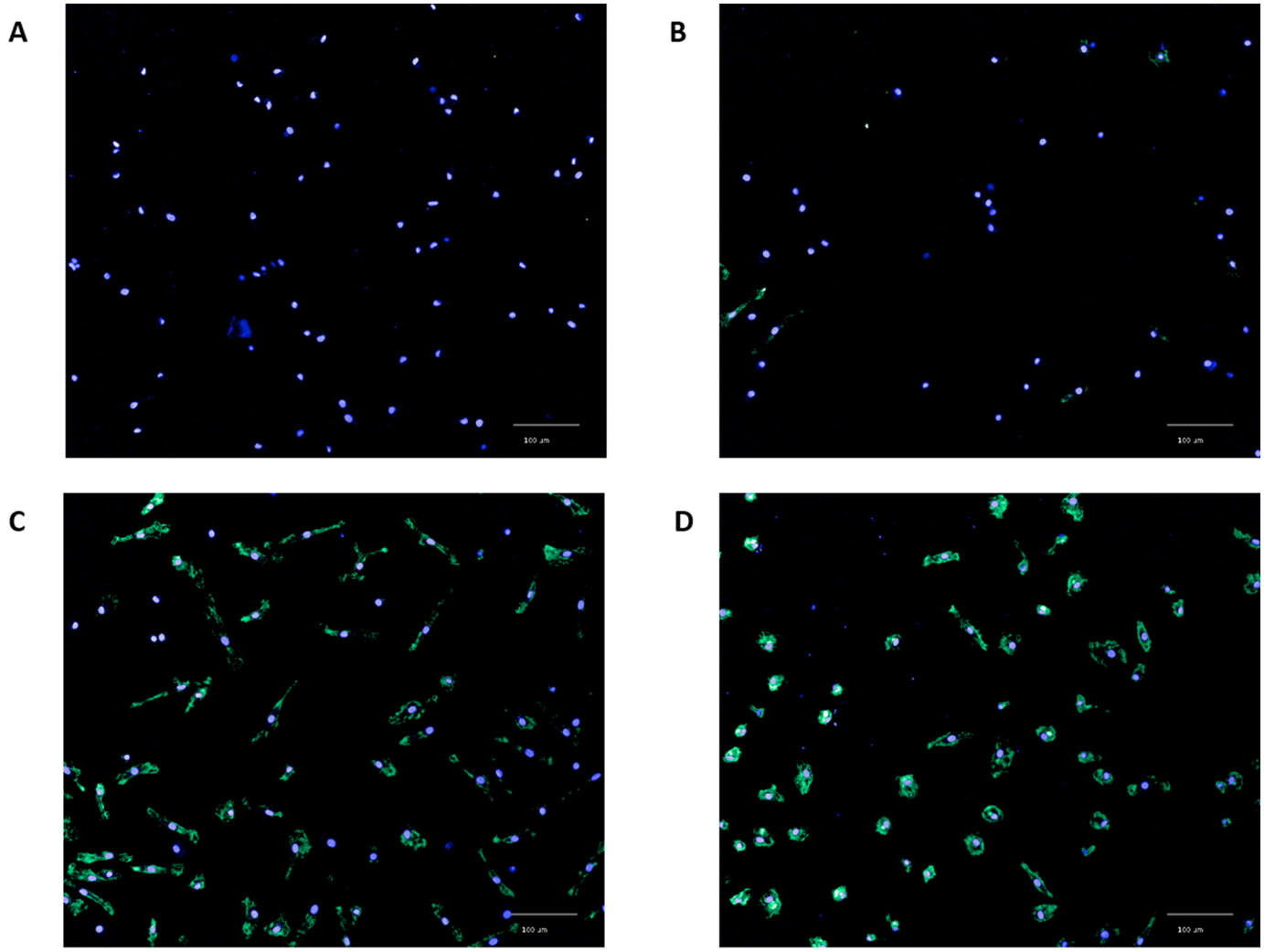

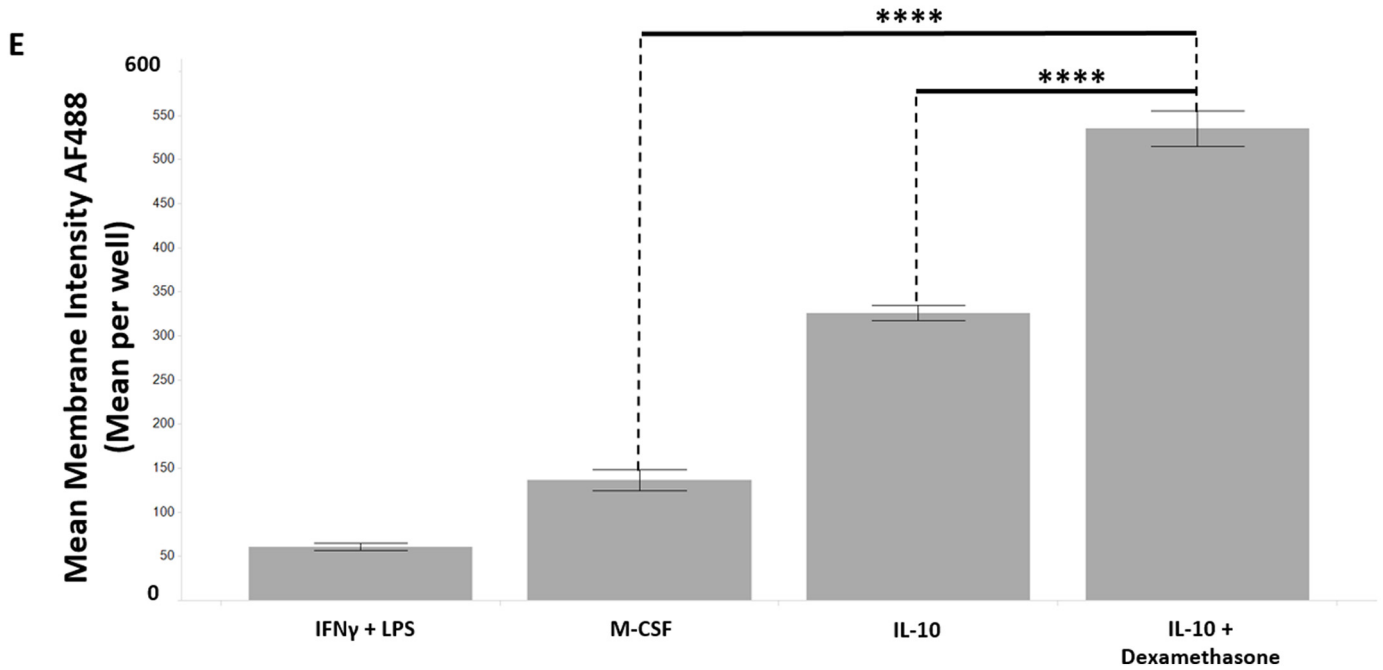

(caption on next page)

Fig. 2. Confocal images of CD14+ monocytes differentiated for 4 days and polarised for an additional 2 days – as defined in methods 2.3 – with either: (**A**) IFNγ + LPS, (**B**) M-CSF, (**C**) IL-10, (**D**) IL-10 + Dexamethasone. Images were acquired at 20× magnification on a CV7000S plate-based imager and show nuclei (Blue) defined by Hoechst and MerTK (Green) defined by rabbit anti-human MerTK antibody (CST #D21F11) used at 1:500 dilution + Alexa Fluor 488 (AF488) donkey anti-rabbit (Invitrogen #A21206) used at 1:1000 dilution. Contrast is set globally across all images and therefore relative intensity can be qualitatively compared. Scale bars shown on each image denote a 100 μm distance. (**E**) Quantification of membrane AF488 intensity calculated via *Columbus* image analysis across $n = 4$ experiments. (For interpretation of the references to colour in this figure legend, the reader is referred to the web version of this article.)

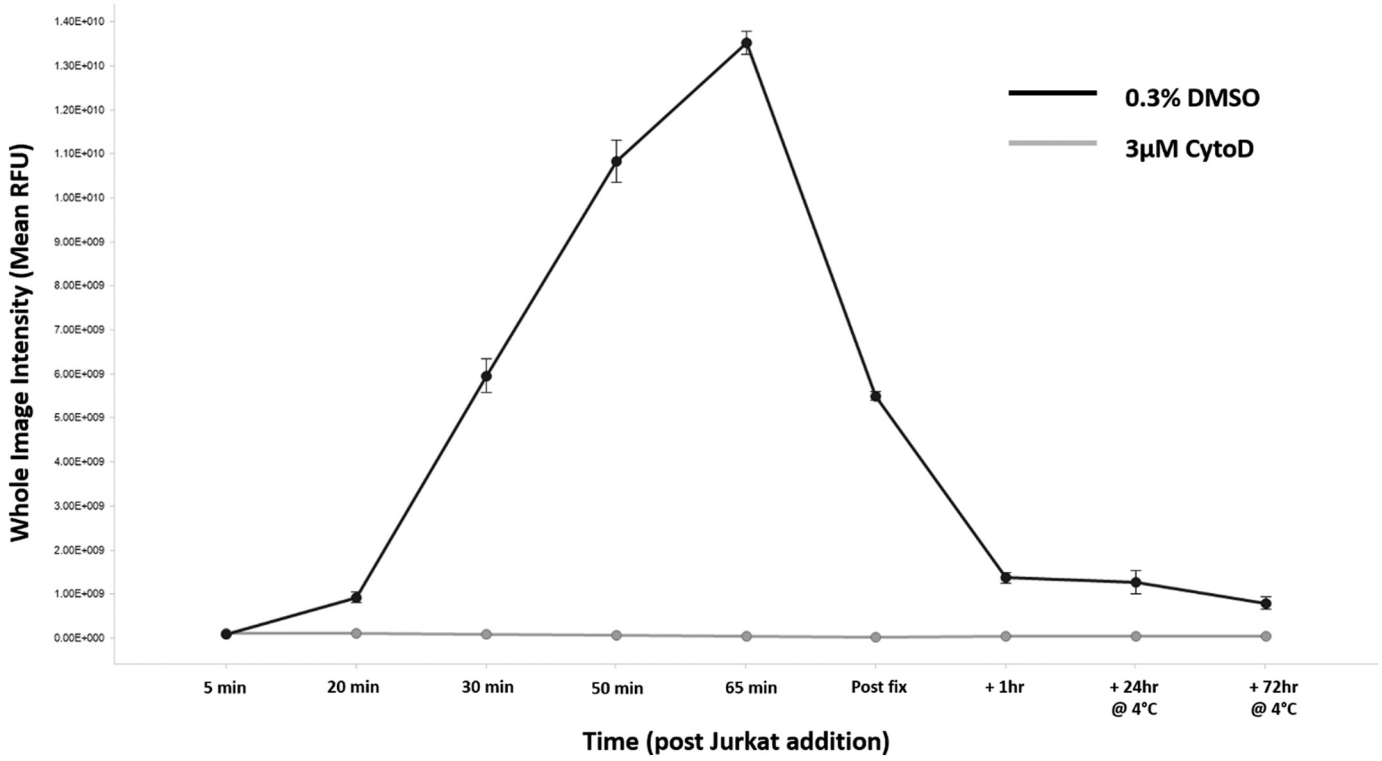

Fig. 3. Change in 'whole-well fluorescence' observed over time across $n = 4$ experiments. Fluorescence intensity observed in Cytochalasin D (CytoD) treated wells remains low over time. The overall fluorescence intensity in DMSO control wells increases rapidly over 60 min, but reduces dramatically upon fixation. Fluorescence intensity remains stable if stored at 4 °C for up to 4 days.

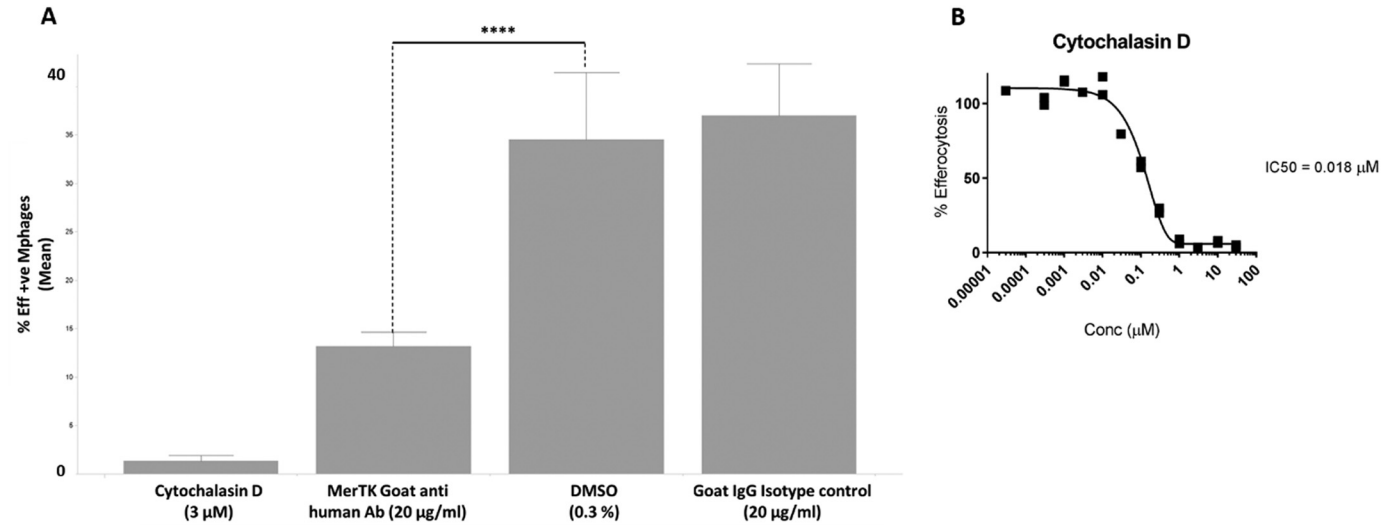

Fig. 4. (**A**) Efferocytosis ability of the CD14+ derived macrophages is inhibited by MerTK antibody. Data shown is across $n = 12$ experiments, using a 1 h incubation time of CytoD or test compound + 1 h incubation with pHrodo-stained Jurkat cells. (**B**) Efferocytosis is also inhibited in a dose-dependent manner by Cytochalasin D (a potent inhibitor of actin polymerisation).

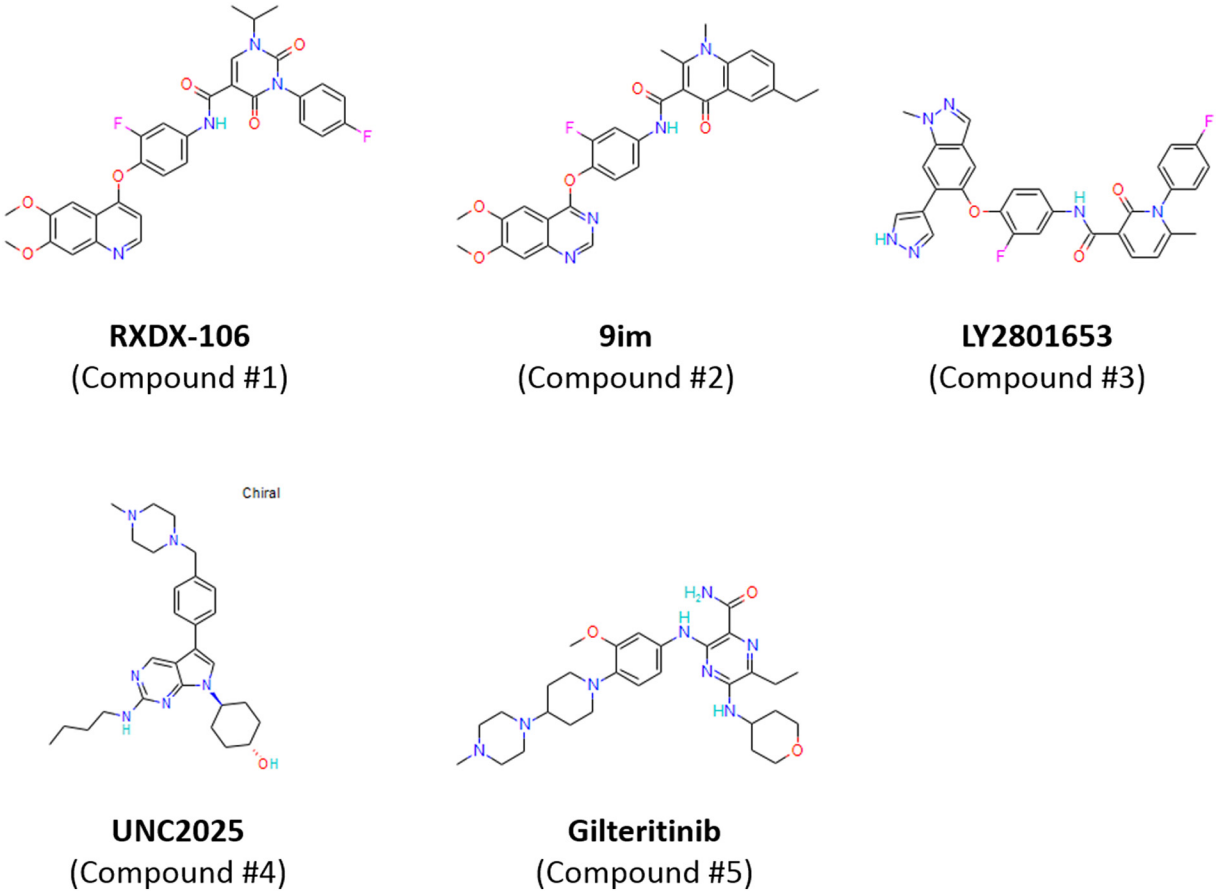

Fig. 5. Various small molecules used to validate the assay (compound #1–4 with claimed MerTK activity along with varying degrees of activity against the related targets AXL, Tyro3, FLT3, c-MET). Compound #5 is claimed as AXL/FLT3 activity only.

Table 1
Activity of the 5 compounds shown in Fig. 5 against 3 key end-points within the assay. Compound #6 is an undisclosed AstraZeneca compound. The data shown relates to the fixed-cell assay with features generated as described in methods 2.9.

Compound	Efferocytosis IC50 (μM)	Macrophage morphology LEC (μM)	Cell number IC50 (μM)
#1	0.004	> 30	> 30
#2	0.049	> 30	> 30
#3	0.073	> 30	> 30
#4	0.04	> 30	> 30
#5	27.1	> 30	> 30
#6	1.83	0.739	> 30
CytoD	0.018	0.002	> 30

cells without them being engulfed). This is a phenomenon that could be anticipated with other test compounds, driving similar phenotypic effects, and should be confirmed through fixation and subsequent image acquisition / analysis at higher magnification in the fixed end-point assay configuration. As can be seen from the macrophage segmentation masks in the fixed cell assay format (Fig. 6, S3, S4, S5) tuning this part of the algorithm to ensure different macrophage morphologies can be accurately segmented is critical to ensure an accurate quantification of true Jurkat uptake.

5. Discussion

We have developed a robust and flexible 384 microplate based high content imaging assay for the functional characterisation of compound effect on human primary monocyte-derived macrophages. The 384 microplate format described here makes this assay suitable for profiling a large number of compounds per assay plate across a concentration range, ensuring that we can maximise the data achieved from the precious primary human cells. Monitoring the assay performance over a number of experimental occasions (spread over many months) we have shown that variability of repeat compound IC_{50} values is very low (Fig. 8). Measuring Robust Z' as an indicator of assay quality over that same time period (Zhang et al., 1999), we routinely achieve values > 0.5 making this assay well suited to continuous profiling of compounds in either efficacy or in-vitro safety settings.

Whilst the majority of the data presented in this manuscript refers to the fixed end-point assay, we have also run the assay in live-cell mode to generate data over a time course (both for assay development purposes and for future expansion of the methodology to explore cytokine profiling following treatment with test compound (Fig. 9)). The ability of the *CV7000S* imager to acquire an entire well in a single field of view, using the 4× objective, was fundamental to enabling this configuration of the assay – acquiring all 384 wells on a plate within 5 min and therefore ensuring minimal assay 'drift' between the starting and ending well on a given plate. Combining this approach with sensitive low volume technologies for detection of cytokine levels has shown some promise (un-published data) and is an area where we would expect this assay could be expanded further in the future.

We have shown that the assay described here carries an advantage over previously published efferocytosis assays (the majority of which are flow cytometry based) in that it can report features related to cell morphology along with the functional effect on efferocytosis. The use of a cryopreserved bank of apoptotic target cells improves robustness and consistency in the assay with good Robust Z' values for a primary cell 384 microplate assay (consistently > 0.5). Using the confocal imaging

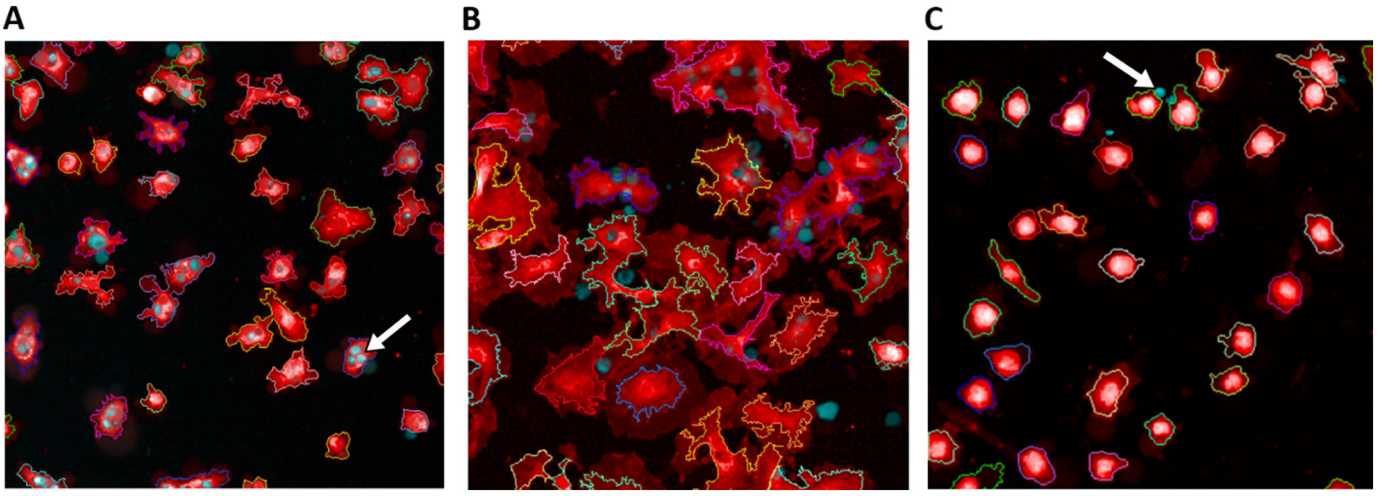

Fig. 6. Confocal images of fixed CD14+ derived macrophages, following 1 h incubation with test compound +1 h incubation with apoptotic Jurkat cells. In all images, macrophages are stained with CellTracker (Red) and apoptotic Jurkat cells with pHrodo (Blue). Segmentation masks applied by *Columbus* are shown. (**A**) Neutral control (0.3% DMSO). Arrow highlights engulfed Jurkat cells. (**B**) Compound #6 at 10 μM. (**C**) Inhibitor control (CytoD at 10 μM). Arrow highlights Jurkat cells on cell surface – outside of segmentation mask. (For interpretation of the references to colour in this figure legend, the reader is referred to the web version of this article.)

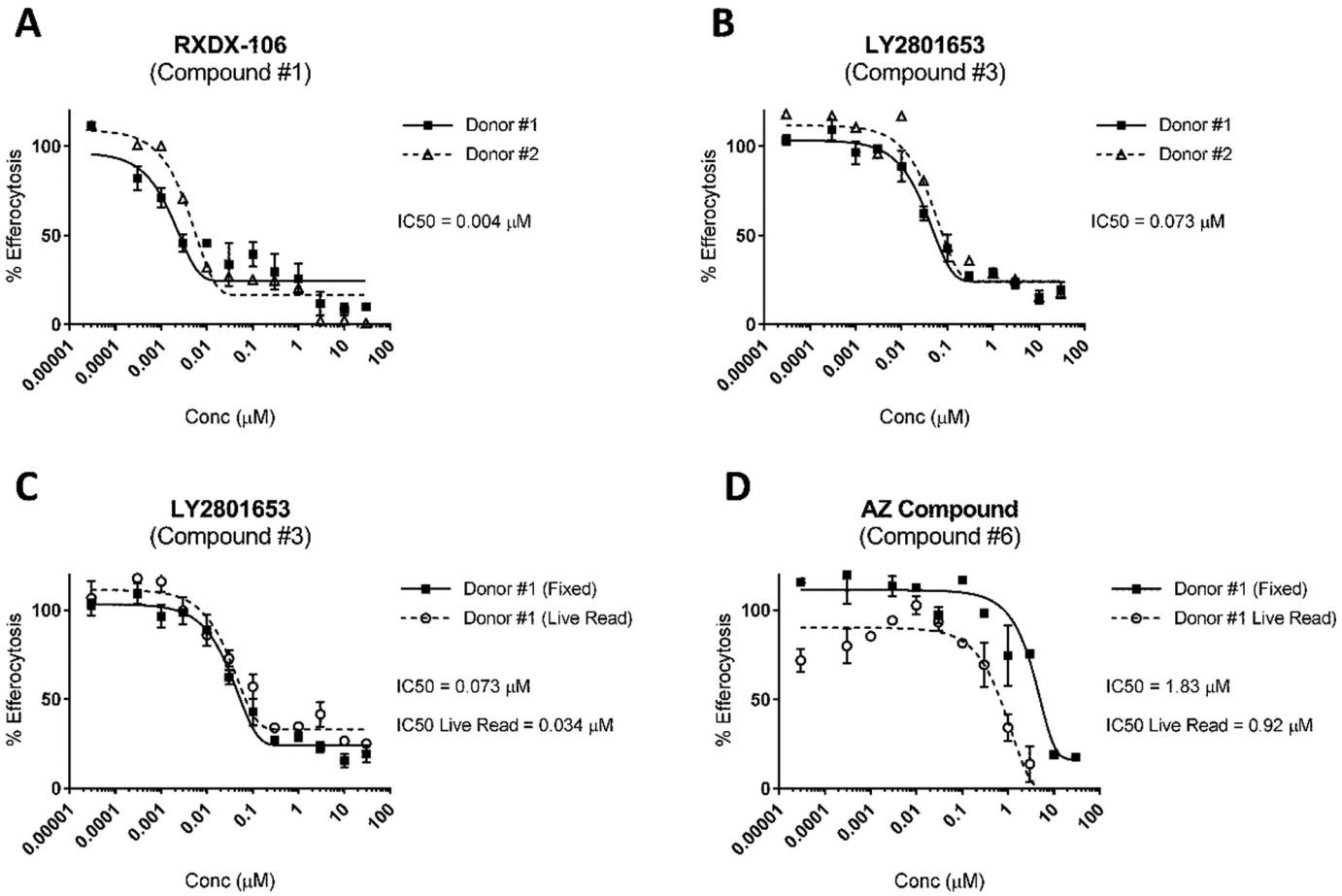

Fig. 7. Concentration response curves generated within the fixed end-point assay. Points shown are mean values over replicates with error bars showing the standard deviation (STDEV) over Donor #1. (**A, B**) Compound #1 and #3 shown across 2 different CD14+ donors. (**C, D**) Comparison of curves generated from donor #1 in either the live-cell or fixed end-point assay (as described in the methods section).

ability of the *CV7000S* to acquire a single *Z*-plane (slicing through the middle of the macrophages) allows the detection of only those target cells which have been internalised by the macrophages – with further removal of any background signal related to partly engulfed or surface-bound target cells possible due to the pH-dependent nature of the target-cell stain. Combining this with the powerful image analysis capability of PerkinElmer *Columbus* enables robust segmentation of the differing macrophage morphologies, and integrating this directly with

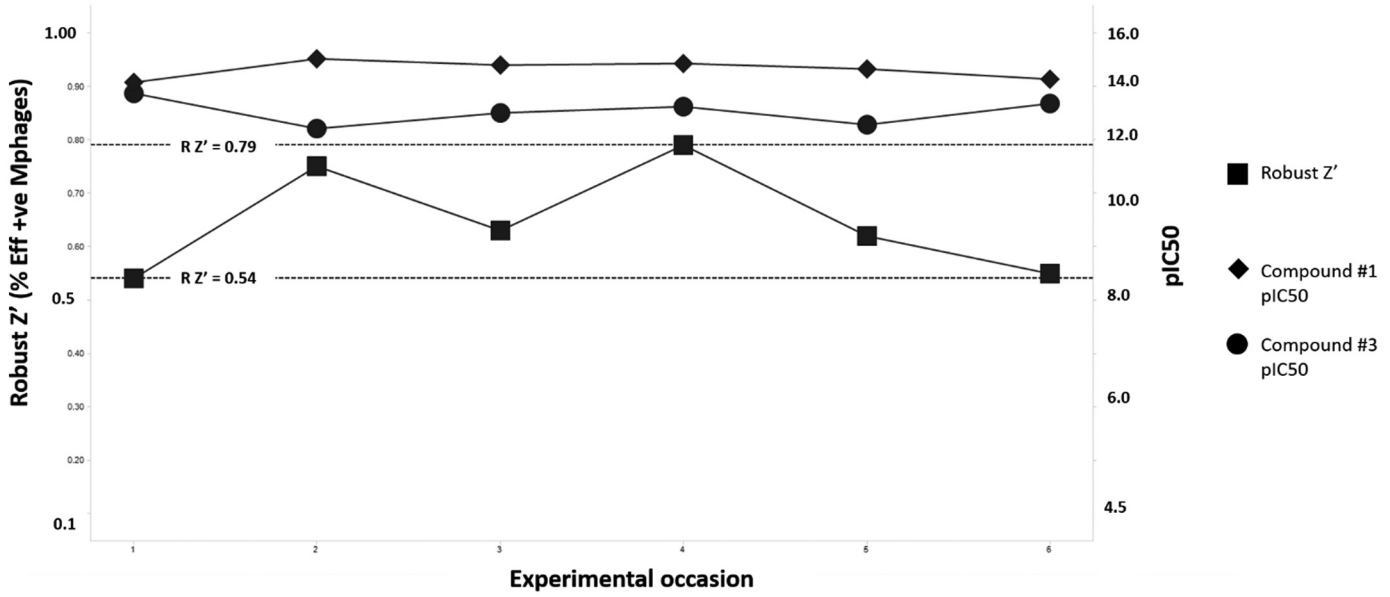

Fig. 8. Assay robustness over multiple experimental occasions. Experiments #1–4 used CD14+ monocytes from donor #1. Experiments #5–6 used CD14+ monocytes from donor #2.

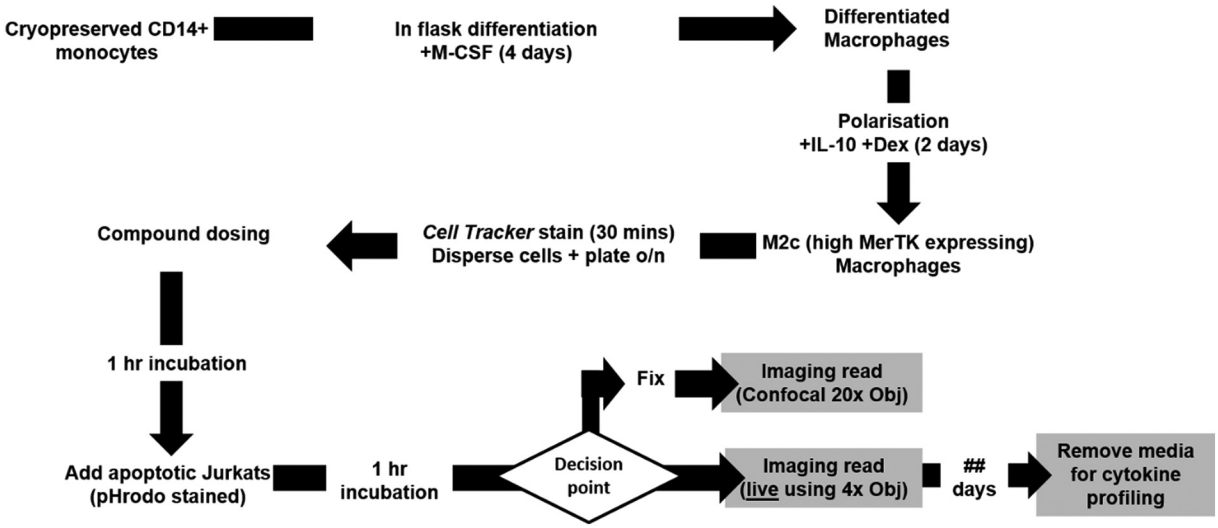

Fig. 9. Assay schematic showing decision-point at image acquisition step (either reading whole-well fluorescence via low magnification objective or PFA fixing cells and taking confocal images over multiple fields via higher magnification objective).

GeneData *Screener*, makes the assay well suited to regular compound profiling workflows.

The fixed-cell assay described here (and shown schematically in Fig. 9) has been routinely deployed within AstraZeneca enabling assessment of compound activity against overall macrophage number, morphological changes and efferocytosis ability. We expect that this methodology could be further expanded by others to enable the study of efferocytosis across different macrophage sub-populations in-vitro (either different polarisation states or indeed across primary macrophages isolated from healthy vs. diseased patient groups).

Funding

This work was funded solely by AstraZeneca.

Declaration of Competing Interest

The authors declare no potential conflicts of interest with respect to the research, authorship, and/or publication of this article.

Acknowledgements

We thank Dr. Yumeng Mao, Dr. Elizabeth Hardaker and Dr. Nadia Luheshi for their help and guidance around all areas of myeloid biology. We thank Dr. William McCoull for his assistance in selection of the validation compounds shown in this manuscript. We thank Mrs. Maelle Mairesse for her assistance in generating the flow cytometry data. We also thank Dr. James Robinson for his help in generation of unpublished supporting material that aided the assay development process.

Appendix A. Supplementary data

Supplementary data to this article can be found online at https://doi.org/10.1016/j.jim.2019.112636.

References

Caron, E., Hall, A., 1998. Identification of two distinct mechanisms of phagocytosis controlled by different rho GTPases. Science (New York, N.Y.) 282 (5394), 1717–1721.

D'Cruz, P.M., Yasumura, D., Weir, J., Matthes, M.T., Abderrahim, H., LaVail, M.M., Vollrath, D., 2000. Mutation of the receptor tyrosine kinase gene Mertk in the retinal dystrophic RCS rat. Hum. Mol. Genet. 9 (4), 645–651.

Duncan, J.L., LaVail, M.M., Yasumura, D., Matthes, M.T., Yang, H., Trautmann, N., Chappelow, A.V., Feng, W., Earp, H.S., Matsushima, G.K., Vollrath, D., 2003. An RCS-like retinal dystrophy phenotype in Mer knockout mice. Invest. Ophthalmol. Vis. Sci. 44 (2), 826–838.

Gal, A., Li, Y., Thompson, D.A., Weir, J., Orth, U., Jacobson, S.G., Apfelstedt-Sylla, E., Vollrath, D., 2000. Mutations in MERTK, the human orthologue of the RCS rat retinal dystrophy gene, cause retinitis pigmentosa. Nat. Genet. 26, 270.

Graham, D.K., Salzberg, D.B., Kurtzberg, J., Sather, S., Matsushima, G.K., Keating, A.K., Liang, X., Lovell, M.A., Williams, S.A., Dawson, T.L., Schell, M.J., Anwar, A.A., Snodgrass, H.R., Earp, H.S., 2006. Ectopic expression of the proto-oncogene Mer in pediatric T-cell acute lymphoblastic leukemia. Clinical Cancer Research 12 (9), 2662–2669.

Graham, D.K., DeRyckere, D., Davies, K.D., Earp, H.S., 2014. The TAM family: phosphatidylserine-sensing receptor tyrosine kinases gone awry in cancer. Nat. Rev. Cancer 14, 769.

Kim, J.E., Kim, Y., Li, G., Kim, S.T., Kim, K., Park, S.H., Park, J.O., Park, Y.S., Lim, H.Y., Lee, H., Sohn, T.S., Kim, K.M., Kang, W.K., Lee, J., 2017. MerTK inhibition by RXDX-106 in MerTK activated gastric cancer cell lines. Oncotarget 8 (62), 105727–105734.

Lemke, G., 2013. Biology of the TAM receptors. Cold Spring Harb. Perspect. Biol. 5 (11), a009076.

Lemke, G., Rothlin, C.V., 2008. Immunobiology of the TAM receptors. Nat. Rev. Immunol. 8 (5), 327–336.

Linger, R.M., Keating, A.K., Earp, H.S., Graham, D.K., 2008. TAM receptor tyrosine kinases: biologic functions, signaling, and potential therapeutic targeting in human cancer. Adv. Cancer Res. 100, 35–83.

Linger, R.M.A., Cohen, R.A., Cummings, C.T., Sather, S., Migdall-Wilson, J., Middleton, D.H.G., Lu, X., Barón, A.E., Franklin, W.A., Merrick, D.T., Jedlicka, P., DeRyckere, D., Heasley, L.E., Graham, D.K., 2013. Mer or Axl receptor tyrosine kinase inhibition promotes apoptosis, blocks growth, and enhances Chemosensitivity of human non-small cell lung Cancer. Oncogene 32 (29), 3420–3431.

Mahajan, N.P., Earp, H.S., 2003. An SH2 domain-dependent, phosphotyrosine-independent interaction between Vav1 and the Mer receptor tyrosine kinase: a mechanism for localizing guanine nucleotide-exchange factor action. J. Biol. Chem. 278 (43), 42596–42603.

Minson, K.A., Smith, C.C., Lee-Sherick, A.B., DeRyckere, D., Lasater, E., Hill, A.A., Wang, X., Frye, S.V., Earp, H.S., Shah, N.P., Graham, D.K., 2014. MRX2843, a novel dual MerTK-FLT3 inhibitor with activity against resistance-conferring FLT3 mutations in acute myeloid Leukemia. Blood 124 (21), 3757.

Mori, M., Kaneko, N., Ueno, Y., Yamada, M., Tanaka, R., Saito, R., Shimada, I., Mori, K., Kuromitsu, S., 2017. Gilteritinib, a FLT3/AXL inhibitor, shows antileukemic activity in mouse models of FLT3 mutated acute myeloid leukemia. Investig. New Drugs 35 (5), 556–565.

Mosser, D.M., Edwards, J.P., 2008. Exploring the full spectrum of macrophage activation. Nat. Rev. Immunol. 8, 958.

Sandahl, M., Hunter, D.M., Strunk, K.E., Earp, H.S., Cook, R.S., 2010. Epithelial cell-directed efferocytosis in the post-partum mammary gland is necessary for tissue homeostasis and future lactation. BMC Dev. Biol. 10 (1), 122.

Santulli-Marotto, S., Gervais, A., Fisher, J., Strake, B., Ogden, C.A., Riveley, C., Giles-Komar, J., 2015. Discovering molecules that regulate Efferocytosis using primary human macrophages and high content imaging. PLoS One 10 (12), e0145078.

Schlegel, J., Sambade, M.J., Sather, S., Moschos, S.J., Tan, A.-C., Winges, A., DeRyckere, D., Carson, C.C., Trembath, D.G., Tentler, J.J., Eckhardt, S.G., Kuan, P.-F., Hamilton, R.L., Duncan, L.M., Miller, C.R., Nikolaishvili-Feinberg, N., Midkiff, B.R., Liu, J., Zhang, W., Yang, C., Wang, X., Frye, S.V., Earp, H.S., Shields, J.M., Graham, D.K., 2013. MERTK receptor tyrosine kinase is a therapeutic target in melanoma. J. Clin. Invest. 123 (5), 2257–2267.

Scott, R.S., McMahon, E.J., Pop, S.M., Reap, E.A., Caricchio, R., Cohen, P.L., Earp, H.S., Matsushima, G.K., 2001. Phagocytosis and clearance of apoptotic cells is mediated by MER. Nature 411, 207.

Shao, W.-H., Zhen, Y., Rosenbaum, J., Eisenberg, R.A., McGaha, T.L., Birkenbach, M., Cohen, P.L., 2010. A protective role of Mer receptor tyrosine kinase in nephrotoxic serum-induced nephritis. Clin. Immunol. 136 (2), 236–244.

Sun, B., Qi, N., Shang, T., Wu, H., Deng, T., Han, D., 2010. Sertoli cell-initiated testicular innate immune response through toll-like receptor-3 activation is negatively regulated by Tyro3, Axl, and Mer receptors. Endocrinology 151 (6), 2886–2897.

Tan, L., Zhang, Z., Gao, D., Luo, J., Tu, Z.C., Li, Z., Peng, L., Ren, X., Ding, K., 2016. 4-Oxo-1,4-dihydroquinoline-3-carboxamide derivatives as new Axl kinase inhibitors. J. Med. Chem. 59 (14), 6807–6825.

Tibrewal, N., Wu, Y., D'Mello, V., Akakura, R., George, T.C., Varnum, B., Birge, R.B., 2008. Autophosphorylation docking site Tyr-867 in Mer receptor tyrosine kinase allows for dissociation of multiple signaling pathways for phagocytosis of apoptotic cells and down-modulation of lipopolysaccharide-inducible NF-kappaB transcriptional activation. J. Biol. Chem. 283 (6), 3618–3627.

Wang, N., Liang, H., Zen, K., 2014. Molecular mechanisms that influence the macrophage m1-m2 polarization balance. Front. Immunol. 5, 614.

Xie, S., Li, Y., Li, X., Wang, L., Yang, N., Wang, Y., Wei, H., 2015. Mer receptor tyrosine kinase is frequently overexpressed in human non-small cell lung cancer, confirming resistance to erlotinib. Oncotarget 6 (11), 9206–9219.

Xu, W., Roos, A., Schlagwein, N., Woltman, A.M., Daha, M.R., van Kooten, C., 2006. IL-10–producing macrophages preferentially clear early apoptotic cells. Blood 107 (12), 4930–4937.

Yan, S.B., Peek, V.L., Ajamie, R., Buchanan, S.G., Graff, J.R., Heidler, S.A., Hui, Y.H., Huss, K.L., Konicek, B.W., Manro, J.R., Shih, C., Stewart, J.A., Stewart, T.R., Stout, S.L., Uhlik, M.T., Um, S.L., Wang, Y., Wu, W., Yan, L., Yang, W.J., Zhong, B., Walgren, R.A., 2013. LY2801653 is an orally bioavailable multi-kinase inhibitor with potent activity against MET, MST1R, and other oncoproteins, and displays anti-tumor activities in mouse xenograft models. Investig. New Drugs 31 (4), 833–844.

Zhang, J.H., Chung, T.D., Oldenburg, K.R., 1999. A simple statistical parameter for use in evaluation and validation of high throughput screening assays. J. Biomol. Screen. 4 (2), 67–73.

Zizzo, G., Hilliard, B.A., Monestier, M., Cohen, P.L., 2012. Efficient clearance of early apoptotic cells by human macrophages requires M2c polarization and MerTK induction. J. Immunol. 189 (7), 3508–3520.